

Revisiting defect-induced magnetism in graphite through neutron irradiation

Yutian Wang,^{1,2} Pascal Pochet,^{3,4} Catherine A. Jenkins,⁵ Elke Arenholz,⁵ Gregor Bukalis,⁶ Sibylle Gemming,^{1,7,8} Manfred Helm,^{1,2,8} and Shengqiang Zhou¹

¹*Helmholtz-Zentrum Dresden-Rossendorf, Institute of Ion Beam Physics and Materials Research, P.O. Box 510119, 01314 Dresden, Germany*

²*Technische Universität Dresden, 01062 Dresden, Germany*

³*Univ. Grenoble Alpes, INAC-SP2M, L_Sim, F-38000 Grenoble, France*

⁴*CEA, INAC-SP2M, Atomistic Simulation Lab., F-38000 Grenoble, France*

⁵*Advanced Light Source, Lawrence Berkeley National Laboratory, Berkeley, California 94720, USA*

⁶*Helmholtz-Zentrum Berlin für Materialien und Energie, Lise-Meitner-Campus, Hahn-Meitner-Platz 1, 14109 Berlin, Germany*

⁷*Faculty of Science, Technische Universität Chemnitz, 09107 Chemnitz, Germany*

⁸*Center for Advancing Electronics Dresden, Technische Universität Dresden, 01314 Dresden, Germany*

We have investigated the variation in the magnetization of highly ordered pyrolytic graphite (HOPG) after neutron irradiation, which introduces defects in the bulk sample and consequently gives rise to a large magnetic signal. We observe strong paramagnetism in HOPG, increasing with the neutron fluence. The induced paramagnetism can be well correlated with structural defects by comparison with density-functional theory calculations. In addition to the in-plane vacancies, the trans-planar defects also contribute to the magnetization. The lack of any magnetic order between the local moments is possibly due to the absence of hydrogen/nitrogen chemisorption, or the magnetic order cannot be established at all in the bulk form.

I. INTRODUCTION

Defect induced magnetism in carbon based materials gives many attractive perspectives in the fundamental understanding of magnetism as well as in future spintronic applications. As early as 2003 highly ordered pyrolytic graphite (HOPG) was reported to be ferromagnetic after proton irradiation¹, which provides an approach to control the defect-induced magnetism in graphite both concerning strength and in lateral distribution. After that, successive investigations were performed for testing the reliability of the ferromagnetism in graphite²⁻⁹ and for finding other carbon-based ferromagnetic materials¹⁰⁻¹⁵. As a consequence, the investigation on defect induced magnetism in semiconductors has been greatly stimulated¹⁶⁻²¹. So far experiments and theory show the following common features:

1. Paramagnetism can be greatly enhanced by introducing defects in graphite or graphene²²⁻²⁴. Some research groups conclude that these paramagnetic centers do not show any magnetic ordering down to 1.8 or 2 K²³⁻²⁵.
2. Ferromagnetism only appears under certain defect concentrations, i.e., in a narrow ion fluence window, and the magnetization is weak^{17,20,22,26,27}.
3. In a microscopic picture, it has been found both theoretically²⁸ and experimentally^{26,29} that defect-induced or disturbed electron states play an important role in generating local moments in graphite.
4. Foreign (or impurity) atoms, particularly, hydrogen and nitrogen, are helpful in establishing the ferromagnetic coupling between defects^{28,30,31}.

However, as to our knowledge, the research has focused mostly on thin-film like samples: ion implanted graphite with nm- μ m affected thickness or graphene flakes. The as-measured magnetization is always in the range of 10^{-6} - 10^{-5} emu per sample^{1,17,20-22,26}. The small magnetization renders data interpretation controversial as shown in a recent intensive discussion on the potential contamination in graphite³²⁻³⁷ as well as on artificial effects in magnetometry^{38,39}. Moreover, the implanted ions, especially those that differ chemically from the substrate, will stay in the matrix as foreign atoms and an interface will naturally form between the implanted region and the untouched substrate. Both the interface and the implanted ions will make it difficult to unambiguously identify the defect type and hamper the interpretation of the mechanism for the observed magnetization. To avoid these problems we use neutron irradiation. Neutrons have a much stronger penetrating capability than ions and will generate defects throughout the whole sample. In this way, the foreign ion effect and the interface effect can be excluded in the present study. Therefore, the application of neutron irradiation could be a promising method to clarify the long standing question regarding the origin of the defect induced magnetism in graphite in the following aspects.

- To verify whether the defect induced paramagnetism or ferromagnetism is a bulk effect or only a surface effect;
- To make a correlation between magnetism and defects based on the strong magnetic signal and results from various structural analysis techniques.

Accordingly, our work has been performed in the following way. HOPG specimens were subjected to neutron irradiation, whereby the irradiation fluence is varied to

induce defects in graphite from slight damage to near amorphization. The magnetic and structural properties have been measured by various techniques. The results were complemented with a theoretical interpretation of the role of in-plane defects from literature and from new first-principles calculations of magnetic states of trans-planar divacancy configurations.

The paper is organized as follows. In section II all experimental methods employed will be described. Then the results will be presented in three sub-sections. In section III.A, we present the large paramagnetism induced by irradiation and its dependence on the neutron fluence. In section III.B and C, the defect type and its concentration evolution will be discussed based on Raman and X-ray absorption spectroscopy, respectively. In section IV, we attempt to correlate the induced paramagnetic centers with in-plane vacancies and trans-planar defects by reviewing the literature data as well as by first-principles calculations. In the end of the discussion section, we also explain why the magnetic coupling between the induced moments is missing. The paper is finished with a short conclusion.

II. EXPERIMENTAL METHODS

In the experiment, the used graphite samples were highly oriented pyrolytic graphite (HOPG) with a grade of ZYA, which are generally referred as graphite in this manuscript. Neutron irradiation was performed at the reactor BER II (Position DBVK) at Helmholtz-Zentrum Berlin⁴⁰. During irradiation the temperature of the samples was less than 50 °C (see ref. 41). Four samples were irradiated with the fluences of 6.24×10^{17} , 1.25×10^{18} , 6.24×10^{18} , and $3.12 \times 10^{19} \text{ cm}^{-2}$, which are named as 3H, 6H, 30H and 150H according to the irradiation time of 3 hours, 6 hours, 30 hours, 150 hours, respectively. The mechanism to produce crystal lattice defects by neutron irradiation is the elastic or inelastic scattering between neutrons and target nuclei. If the target nucleus gets enough energy after scattering, it will irreversibly displace the lattice atom from its original site, resulting in vacancies and interstitials. The minimum energy required to displace a carbon atom in graphite is around 25 eV⁴². Therefore, we only consider the epithermal (0.5 eV – 100 keV) and fast neutrons (100 keV – 20 MeV)⁴³ in calculating the fluence. The elastic scattering dominates when the energy is below 5.5 MeV in carbon and the nuclear reaction (inelastic scattering) only becomes appreciable when the energy is above 9 MeV⁴².

Magnetometry was performed using a SQUID-VSM (Quantum Design). The magnetic properties were measured regarding their dependences on magnetic field and on temperature. The structure change is characterized by Raman spectroscopy which is sensitive to defects in the aromatic ring, the edge state, the hybridization type, the interstitial ions, and also to the stacking orders, etc⁴⁴. The μ -Raman system is equipped with a 532 nm wave-

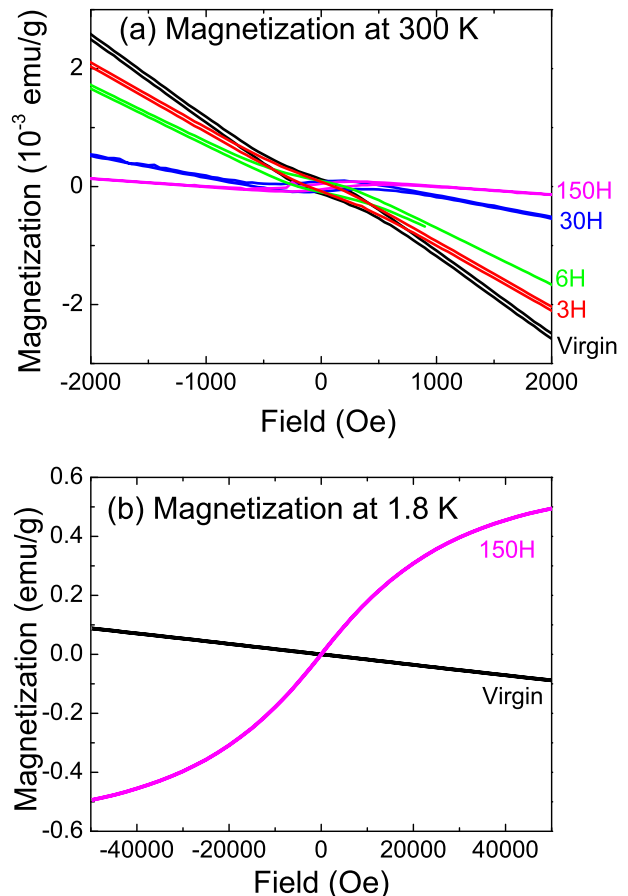


FIG. 1. Magnetization vs. field (a) the low field range at 300 K and (b) the large field range at 1.8 K.

length laser and a liquid nitrogen cooled CCD detector working in backscattering geometry. X-ray absorption spectroscopy (XAS) will further detect the bonding state change resulting from neutron irradiation. The variations of the magnetization, the Raman scattering and the X-ray absorption at the carbon K-edge depending on the irradiation fluence allow us to clearly correlate the density of vacancies interstitials with the magnetism in the neutron irradiated graphite.

III. RESULTS AND DISCUSSION

A. Magnetic properties

Figure 1 shows the magnetization measurements at 300 K and 1.8 K for the virgin and irradiated graphite without any background correction. For the virgin graphite, the diamagnetic background dominates the magnetic properties. A weak ferromagnetic hysteresis is observed already in the virgin graphite. It is probably caused by

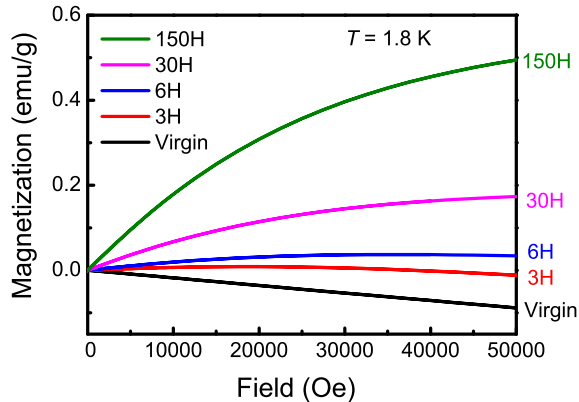


FIG. 2. The magnetic moments of all irradiated sample measured at 1.8 K as a function of the applied external field.

intrinsic defects³⁰ or by Fe contamination^{33,34,37}. Moreover, the ferromagnetic contribution is not changed significantly upon neutron irradiation. Therefore, this weak ferromagnetism is not the topic of our study in this manuscript. Besides the marginal change in the ferromagnetic component, there is a huge increment of the magnetization at low temperature. Figure 1(b) shows the comparison of the magnetization measurement at 1.8 K for the virgin graphite and sample 150H. Sample 150H shows a large paramagnetic component which will be discussed in detail later. Note that the change in the slope of the MH curves in Fig. 1(a) is due to the large increase of the paramagnetism upon irradiation as shown. At low temperature, the weak ferromagnetism in the irradiated samples is dominated by the paramagnetism and not resolvable.

The field dependence of the magnetization at 1.8 K for all samples is shown in Fig. 2. Neutron irradiation leads to strong paramagnetism. The graphite sample is changed completely from diamagnetic-like to paramagnetic-like with increasing neutron fluence. However, even for the sample with the highest neutron fluence, the magnetization is not saturated at 1.8 K up to a field of 50000 Oe. In our experiment, the measured absolute magnetic moment for a graphite sample of around $4 \times 4 \text{ mm}^2$ is in the range of 0.001-0.01 emu at 1.8 or 5 K. This value is much larger than the previously reported ion implanted samples with a magnetic moment of around 10^{-5} - 10^{-6} emu^{1,17,22,26} and is far above the sensitivity of SQUID-VSM. As shown in Fig. 3(a), the induced paramagnetism can be precisely described by the standard Brillouin function after removing the residual diamagnetic background and the intrinsic paramagnetic contribution from the virgin graphite:

$$M(\alpha) = NJ\mu_B g \left[\frac{2J+1}{2J} \coth\left(\frac{2J+1}{2J}\alpha\right) - \frac{1}{2J} \coth\left(\frac{1}{2J}\alpha\right) \right] \quad (1)$$

where the g factor is about 2 obtained from electron

spin resonance measurement (not shown), μ_B is Bohr magneton, $\alpha = gJ\mu_B H/k_B T$, k_B is the Boltzmann constant and N is the density of spins. The Brillouin function provides excellent fits for $J = 0.5$, which corresponds to single electrons as charge carriers and $N = 8 \times 10^{19} \mu_B/\text{mg}$ for sample 150H. The fits using larger J unequivocally deviate from the shape of the measured M-H curves, as they give significantly different, sharper changes with faster saturation.

The Curie law

$$\chi = \frac{M}{H} = N \frac{J(J+1)(g\mu_B)^2}{3k_B T} \quad (2)$$

with $J = 0.5$ and $N = 8 \times 10^{19} \mu_B/\text{mg}$ inferred from Fig. 3(a) also gives a good fit to the temperature dependent magnetization as shown in Fig. 3(b). The inset of Fig. 3(b) shows the inverse susceptibility versus temperature, revealing a linear, purely paramagnetic behavior with no indication of magnetic ordering.

Figure 6 (shown later in the paper) shows the density of paramagnetic centers obtained by fitting the magnetization measured at 1.8 K for different samples as a function of neutron fluence in double logarithmic scale. With increasing neutron fluence, i.e. the amount of defects, more and more paramagnetic centers are generated. This indicates that even the most strongly irradiated sample is still not totally amorphous.

We also noted the work by Ramos et al.²² Using ion implantation to introduce defects into graphite, they reported an anomalous paramagnetic contribution. This contribution remains independent of temperature up to 100 K, whereas the field dependent magnetization shows neither saturation nor any nonlinearity²². Meanwhile theoretical calculations also pointed out that if sufficient carbon adatoms were available, they could weakly agglomerate in graphene and superparamagnetism can be finally observed⁴⁵. However, in our experiment the magnetic properties for all samples can be well described by spin 1/2 paramagnetism without superparamagnetic contributions. As expected if the whole volume contributes, in our experiment the as-measured magnetization signal is as large as 0.001–0.01 emu per sample. The large magnetization signal allows us to draw reliable conclusions and to exclude any spurious and anomalous paramagnetic contribution.

To further exclude a possible ferromagnetic ordering in our sample we measured the magnetization vs. field at different temperature to perform an Arrott plot analysis⁴⁶. This method is usually used to accurately determine the Curie temperature T_C and to verify the paramagnetic to ferromagnetic phase transition. Such an analysis is based on the relationship derived by Wohlfarth⁴⁷

$$[M(H, T)]^2 = [M(0, 0)]^2 [1 - (T/T_C)^2 + 2\chi_0 H/M(H, T)] \quad (3)$$

Note that this relationship results in parallel lines of the isothermal M^2 which cross zero ($H/M = 0$) in the vicin-

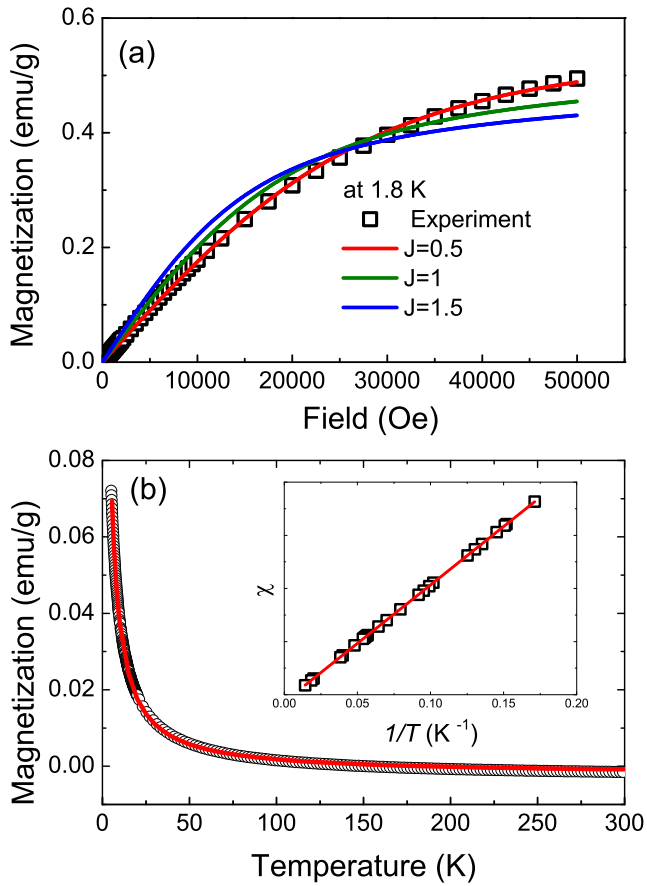


FIG. 3. (a) The measured magnetization at 1.8 K for sample 150H and the fitting using Brillouin function with $J = 0.5, 1, 1.5$. (b) Temperature dependent susceptibility measured under a field of 10000 Oe. The black symbols are experimental data and the red solid curve is the fitting result by the equation (2). Inset: Inverse susceptibility versus temperature demonstrating a linear, purely paramagnetic behavior with no indication of magnetic ordering.

ity of $T = T_C \pm \delta$. Figure 4 shows the isothermal magnetization Arrott plot for sample 150H (irradiated up to the highest fluence). The measurement temperatures range from 1.8 K to 20 K. With increasing temperature, the magnetization decreases, but none of the lines crosses the zero point ($H/M = 0$). It confirms that down to 1.8 K no magnetic order appears in this sample. It is purely paramagnetic.

B. Raman spectroscopy

Figure 5 shows the Raman spectra of graphite samples after neutron irradiation. From top to bottom are the virgin sample and samples 3H...150H, respectively. A linear background has been removed.

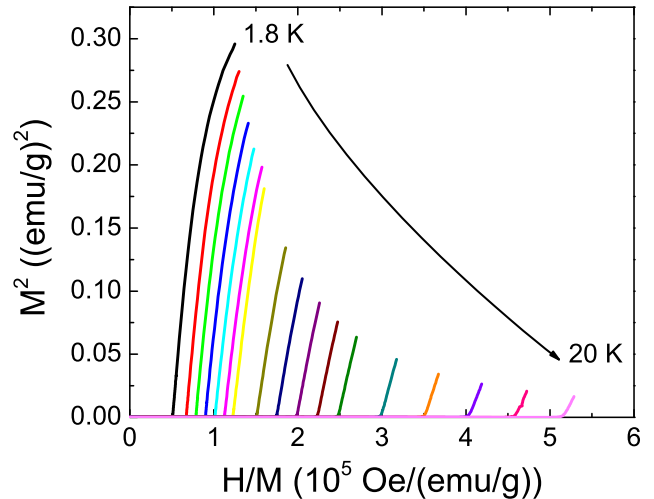


FIG. 4. Isothermal magnetization an Arrott plot: M^2 versus H/M . The lines with different color correspond to the measurements in the temperature range 1.8 to 20 K.

The reference sample shows the peaks typical for the high-quality HOPG^{44,48}. The G peak located at around 1590 cm^{-1} corresponds to the inherent E_{2g} mode of the aromatic ring. The D peak around 1360 cm^{-1} represents an elastic scattering at defects in crystal^{44,48-50}.

Upon neutron irradiation, the most pronounced changes occur in the D peak and in its overtone G' peak (2D peak): the D peak rises with irradiation fluence and becomes as strong as the G peak. Two pronounced changes will be described in the following.

1. In-plane vacancies

The increase of peak D is generally attributed to the in-plane vacancies in graphite^{44,48-50}. By independent methods such as X-ray diffraction and transmission electron microscopy, the intensity ratio between D and G peaks has been confirmed as a measure of the in-plane grain size. Neutron irradiation induces a large number of interstitial and vacancy pairs ($I-V$). Most of $I-V$ defects will recombine simultaneously and the remaining species can form various defects. Since a high energy barrier blocks the diffusion of vacancies, most vacancies become in-plane vacancies or form vacancy clusters. The interstitial atoms prefer staying in the region between the layers owing to the energetically highly unfavorable interstitial in-plane position⁵¹. In Figure 6, we plot the fluence dependent I_D/I_G (the intensity ratio between D and G peaks). In our samples, the strength of the D peak increases with the neutron fluence when the irradiation time is less than 30 hours. Further increasing the neutron fluence, I_D/I_G reaches a saturation value. It indicates that with increasing the irradiation time from

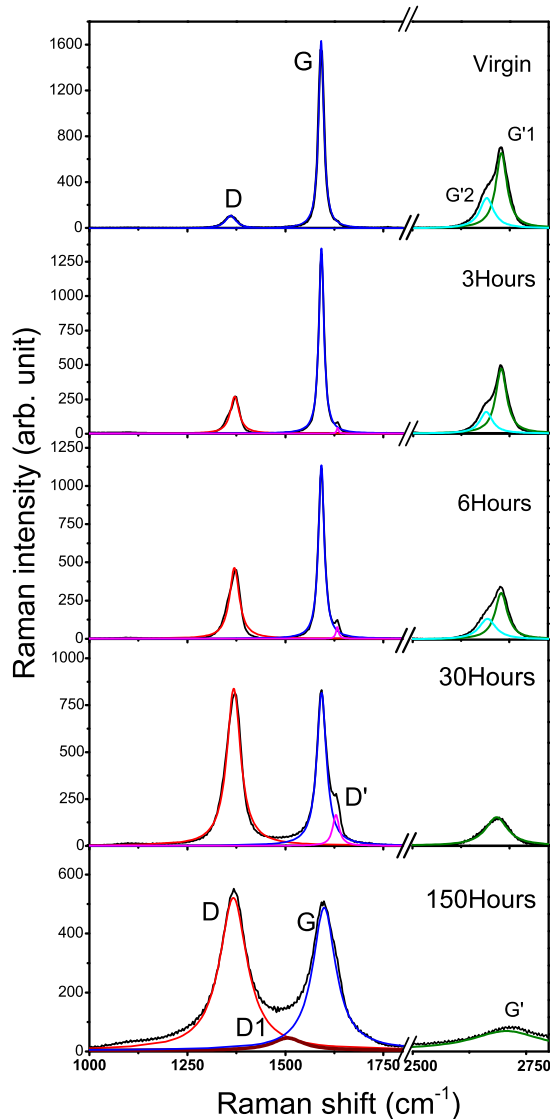


FIG. 5. Raman spectra of graphite after neutron irradiation. From the top to bottom shown are data for virgin graphite and 3 hours to 150 hours irradiated samples, respectively. The peaks were deconvoluted to reveal the detailed variation after neutron irradiation.

3 hours to 30 hours the density of vacancies is continuously increasing until the vacancies reach a saturation density. Such behavior was observed in ion irradiated or ball milled graphite^{49,50}.

2. Out-of-plane defects

The G' peak around 2720 cm^{-1} is the overtone of the D peak. It is often referred as the 2D peak and is very sensitive to the c -axis stacking order of graphite. The line shape and intensity of G' are signatures of the stacking of graphene layers. For bulk graphite consisting of

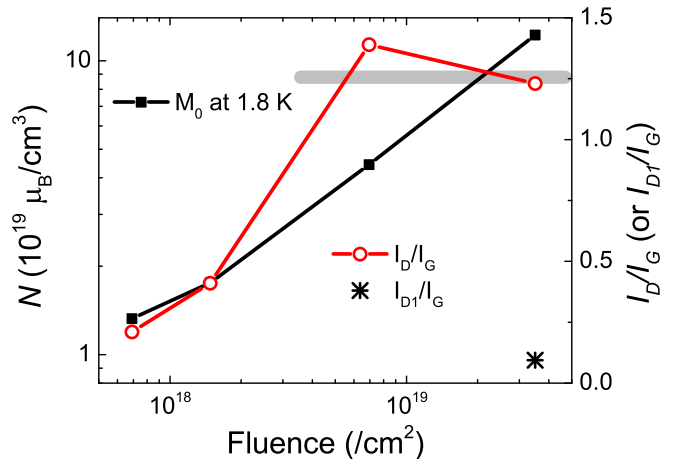


FIG. 6. The intensity ratio between D and G peaks (I_D/I_G) and the fitted paramagnetic center density (N , at 1.8 K) vs. neutron irradiation fluence. The grey bar indicates the saturation value of I_D/I_G for ion implanted graphite⁴⁹.

an $\dots ABAB \dots$ stacking, the G' peak is composed of two peaks. When the stacking is absent, the interaction between the planes is very weak and they behave as two-dimensional crystals. For a single graphene layer, the G' peak is composed of a single peak⁴⁴. For our experiment, in the virgin sample the interaction between the layers in 3D graphite makes the G' peak to be split into $G'1$ and $G'2$. When the irradiation time is less than 6 hours, two peaks can fit the spectra, but their strength becomes weak with increasing irradiation fluence. This indicates a slight crystalline damage in the graphene sheet stacking. The influence of shear moments caused by the interstitial atoms between the two sheets is less notable for irradiation times of less than 6 hours. When the irradiation time is over 30 hours, $G'1$ and $G'2$ peaks decrease strongly and mix into a single weak peak. This is attributed to the out-of-plane defects in graphite^{48,52}. With increasing neutron fluence, more interstitial atoms are assumed to diffuse into regions between the graphene sheets so that the distance between the sheets increases strongly enough, such that the graphene sheets behave like an isolated single graphene sheet. The appearance of the $D1$ peak at around 1500 cm^{-1} for sample 150H is another indication for the interstitial atoms between graphene sheets^{48,53}. At low fluence range, the $D1$ peak is too weak to be fitted even for samples 30H. The $D1$ peak was also observed in ion implanted graphite when the implantation fluence is large enough⁴⁸.

This Raman analysis allows us to define two regimes for the four reported fluences. In the first regime (3H, 6H and 30H) defects are created in plane without interaction between neighboring planes. In the second regime (30H and 150H), the latter interaction becomes a dominant ef-

fect and trans-planar defects (interstitial or vacancy) are expected to play a major role: due to the high defect concentration, newly created defects are expected to combine with pre-existing defects in the neighboring planes as revealed by the rather saturated value of I_D/I_G in the second fluence regime. Interestingly, these transplanar defects seem also contribute to the total magnetization.

C. X-ray absorption spectroscopy

To further probe the change in the electronic state in graphite after neutron irradiation from a microscopic point of view, we performed near-edge X-ray absorption fine structure spectroscopy (NEXAFS, Beamline 6.3.1 at the Advanced Light Source in Berkeley). The description of the experimental set up can be found in reference 30. In our experiment, the incident light was inclined by 45° to the sample surface. The signals were collected in the total electron yield mode at room temperature. All the spectra are normalized by the input flux for comparison.

As shown in Fig. 7, there are two resonances around 285 eV and 292 eV, respectively. They correspond to the transitions from $1s$ core-level electrons to π^* and σ^* empty states, respectively. For samples 3H and 6H with a small neutron fluence, there is no significant change either in the peak intensity or in the peak shape compared with the virgin sample. After the irradiation over 30 hours, the intensity of the π^* peak decreases, which indicates that the aromatic π system is severely perturbed. At the same time, the π^* and σ^* features are becoming broader. In previous literature, it has been shown that the π^* and σ^* resonances of carbon are much more broadened in proton implanted graphite than our case^{30,54}.

The inset of Fig. 7 shows a zoom into the energy range 280–284 eV. Compared with previous results on ion implanted graphite²⁶, the fundamental difference of our sample is the missing of a pre-edge peak at around 282 eV. In ref. 26, a new small, but sizeable peak in the pre-edge region (281.5 eV to 284.5 eV), has been reported in ion implanted ferromagnetic graphite. This new peak was attributed to be closely related with defect states near the Fermi energy level, and it was temporarily assigned to rehybridized C-H bonds. The lack of rehybridized C-H bonds in our samples may explain the absence of ferromagnetism, which will be discussed later.

IV. DISCUSSION

We have investigated the magnetic and structural properties of graphite after neutron irradiation. Different from ion implantation, neutron irradiation can introduce defects in the whole graphite sample. The resulting magnetization is very large and allows one to draw a reliable conclusion free of the influence of contamination. Our experimental results lead to two conclusions: (1) only spin 1/2 paramagnetism is induced in graphite by neutron

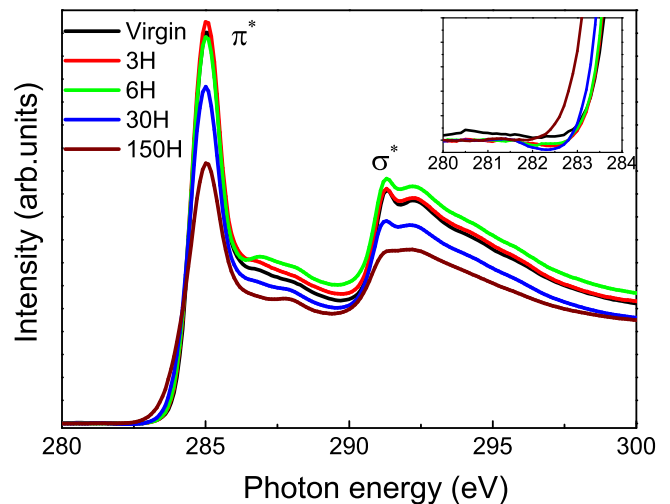


FIG. 7. The NEXAFS spectra of the graphite samples after neutron irradiation for different time. Inset: zoom into the energy range 280–284 eV.

irradiation; and (2) both in-plane vacancies and out-of-plane defects appear after irradiation. In this discussion, we attempt to correlate the magnetization and defects and to understand why the magnetic ordering is lacking.

A. The origin of the paramagnetism

Defect induced magnetism in both graphite and graphene has been intensively investigated theoretically. Structural defects, in general, can give rise to localized electronic states. It is well accepted that the in-plane vacancies are the origin of local magnetic moments²⁴. Upon removal of one atom, each of the three neighboring atoms has one sp^2 dangling bond. Two of the C atoms can form a pentagon, leaving one bond unsaturated. This remaining dangling bond is responsible for the magnetic moment. Moreover, the flat bands associated with defects lead to an increase in the density of states at the Fermi level. Lehtinen et al., used spin-polarized DFT and demonstrated that vacancies in graphite are magnetic⁵⁵. They also found that hydrogen will strongly adsorb at vacancies in graphite, maintaining the magnetic moment of the defect. Zhang et al.²⁸ have confirmed that the local moments appear near the vacancies and with increasing vacancy accumulation the magnetization decreases non-monotonically. Using a combination of a mean-field Hubbard model and first principles calculations, Yazyev also confirmed that vacancies in graphite and graphene can result in net magnetic moments⁵⁶, while the preserved stacking order of graphene layers is shown to be a necessary condition for achieving a finite net magnetic moment of irradiated graphite. In most calculations,

the moment per vacancy is sizeable up to 1–2 μ_B ^{28,55}. Indeed, by scanning tunneling microscopy experiments, Ugeda *et al.* have observed a sharp electronic resonance at the Fermi energy around a single vacancy in graphite, which can be associated with the formation of local magnetic moments²⁹.

In our neutron irradiated graphite, we observed a strong correlation between the magnetization and vacancies. Figure 6 shows the irradiation-fluence dependent magnetization and the values of I_D/I_G of the Raman spectra. At the low fluence regime, the density of magnetic moments shows an excellent correlation with I_D/I_G (the density of in-plane vacancies): both increase monotonically with the fluence. This indicates an agreement with the theoretical calculation: the vacancy in graphite results in local magnetic moment. In the next subsection, we discuss the role of out-of-plane defects.

B. The role of trans-planar defects

As shown in Fig. 6, I_D/I_G reaches its saturation value of around 1.2–1.4 when the neutron fluence is higher. I_D/I_G of 1.2–1.4 is also a threshold of amorphisation in ion irradiated graphite⁴⁹. Despite the saturation in the density of in-plane vacancies, the density of local moments still increases with neutron fluence as shown in Fig. 6. What is the contribution for these additional local magnetic moments? We consider the role of the trans-planar defects. As shown in Fig. 5, for the largest irradiation fluence, $D1$ peaks appears, which has been attributed to the trans-planar defects⁴⁸. In order to assess the experimental findings described in the above sections, we have investigated the possible magnetic state for trans-planar defects.

We start our analysis from the seminal work of Telling *et al.*⁵⁷ who firstly propose the trans-planar divacancy configurations (see Figure 8) that breaks the symmetry rules in graphite. Interestingly, the spin-polarized states for these defects was discussed in the paper but never assessed. In order to answer this question without any artifacts we have decided to run additional spin-polarized calculations in a super-cell which is large enough to avoid elastic effects between neighboring defect images (in-plane). Systems containing 448 atoms per graphene sheets have proven to be reliable to study triangular vacancy clusters in hexagonal boron nitride sheets⁵⁸ and are also used in the present study. Here, two of these sheets with Bernal stacking were considered. The distance between the two sheets was fixed to 6.45 Bohr radii (a_0) for simplifying the treatment of the interlayer. This is achieved by the freezing of the perpendicular displacements in a band close to the edges of the super-cell (pink area in Fig. 8). This treatment allows for a full relaxation both in-plane and out-of-plane of the central part of the super-cell where the defect sits. The PBE exchange and correlation function was chosen as it was found to well reproduce the in-plane relaxations⁵⁹. The

TABLE I. Formation energy (E_f) and energy difference (E_{spin}) between the singlet and triplet states for the three considered divacancies. The values in bracket are corresponding results in ref. 57.

Samples	E_f (eV)	E_{spin} (meV)
V_2 in-plane	7.55 (8.7)	2
V_2^1 trans-planar	13.85 (14.6)	560
V_2^2 trans-planar	12.77 (13.0)	1

BigDFT⁶⁰ code was used to perform DFT calculations within surface boundary conditions⁶¹.

The two trans-planar divacancies V_2^2 and V_2^1 are considered together with the in-plane divacancy V_2 as a reference. The formation energy of the defect is calculated using the chemical potential of carbon in the pristine bilayer system. Singlet and triplet states are obtained by running spin averaged and spin polarized calculations, respectively. The results are summarized in table I. The formation energy of the three defects increases in-line with the initial report of Telling *et al.*⁵⁷. However, important differences arise, underlying the role of the in-plane relaxations that were blocked in the previously used 64 atoms box⁵⁷. Indeed, while the estimated error of about 0.4 eV⁵⁷ holds for the trans-planar vacancies, the difference is much more bigger for V_2 . As a consequence, the energy difference between the two trans-planar divacancies remains in the order of 1.5 eV.

In Table I we also report the singlet to triplet formation energy for each defect. In line with the report of a double bond⁵⁷ for the inter-planar C-C bond (see bond length scale in figure 8), the V_2^2 divacancy is in a singlet state. This situation is different for the V_2^1 divacancy: the inter-planar C-C bond is longer and more twisted, thus preventing further hybridization between the two carbon atoms. As a consequence, the triplet state is stabilized by more than 500 meV with respect to the singlet state. According to Telling *et al.*, the existence of triplet states gives a solid explanation for the observed spin 1/2 paramagnetism.

C. Why is the magnetic interaction missing?

As shown in Fig. 2 and Fig. 6, the paramagnetism in graphite can be strongly enhanced by irradiation induced defects. After irradiation even to the largest fluence, the samples are not fully amorphous and I_D/I_G of around 1.2 corresponds to a planar grain size of 3.5 nm⁴⁹. Why is the magnetic interaction between the generated paramagnetic centers then missing? To answer this question, we first need to estimate the density of defects, i.e. the average distance between adjacent local moments.

Assuming the defects are homogeneously distributed in the sample matrix, we estimate the average distances (r)

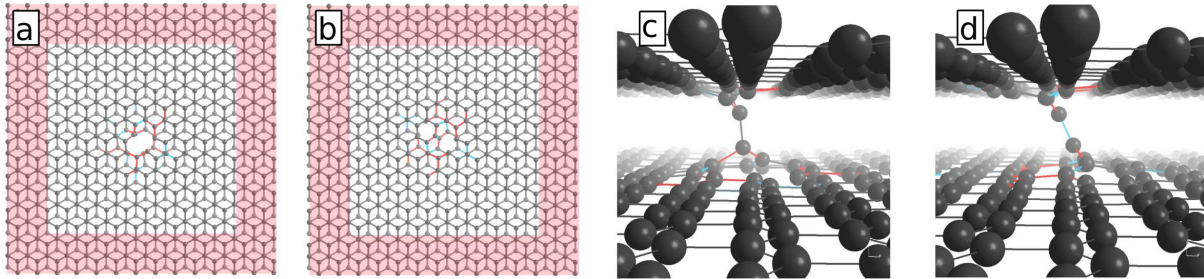


FIG. 8. The top (left) and side (right) view of the two considered trans-planar divacancies: V_1^1 (a, c) and V_2^2 (b, d). Black balls are carbon atoms. Bonds between two neighboring atoms are colored as a function of length: black stands for standard distances [2.70 ± 0.05 Bohr radius (a_0)], blue and red stand for short ($2.60 \pm 0.05 a_0$) and long ($2.80 \pm 0.05 a_0$) distances, respectively.

between local moments in our irradiated graphite samples. This value amounts to 2.2 nm for the sample with the largest neutron fluence. The nearest average distance between two spins is around $16a$ ($a = 0.14$ nm is the C-C bond length). Therefore, the direct coupling between the localized spins at the vacancies is nearly negligible. Alternatively, the Ruderman-Kittel-Kasuya-Yosida (RKKY) coupling is suggested to appear in defective graphite and graphene⁶². This coupling might be ferromagnetic at a finite temperature when $k_F r \ll 1$. If assuming a Fermi energy of 20 meV in graphite⁶³, the inverse of the Fermi wave vector $1/k_F \sim 30$ nm. To have ferromagnetic ordering, the distance between two spins r should be $\ll 30$ nm which corresponds to a spin density of $3.7 \times 10^{18} \text{ cm}^{-3}$. In principle, all samples fulfill this criteria. All these moments may tend to be ferromagnetically coupled via the RKKY coupling, although the Curie temperature can be very low⁶³. However, we do not observe any magnetic ordering down to 1.8 K even for sample 150H. It is not practical to further increase the defect density, since the stacking order of graphenes plane must be preserved^{26,56}. Our sample with the highest neutron fluence is already at the verge of amorphization. A larger irradiation fluence will perturb the graphene lattice too much and destroy the necessary band structure and carrier density.

Both published theory and experimental results suggest a crucial role of hydrogen or nitrogen chemisorption in enhancing the spin density and in establishing the magnetic coupling^{28,30,55,56,63}. All these moments from chemisorption will tend to be ferromagnetically coupled, enhancing the Curie temperature by the RKKY coupling. Recently, by careful angular dependent NEXAFS, He et al. observed a new small peak in the pre-edge region (281.5 eV to 284.5 eV)²⁶. This new peak has been interpreted to be closely related with the defect states near the Fermi energy level and it is assigned to the formation of C-H bonds³⁰. Ohldag et al. also observed an X-ray magnetic circular dichroism (XMCD) signal in the pre-edge region of the C K-edge. However, as shown in Fig.

7, our present findings do not exhibit any new peak in the pre-edge of the C K-edge. This may explain why the ferromagnetic coupling is missing.

V. CONCLUSION

Neutron irradiation in graphite can induce a large amount of defects throughout the bulk specimens, consequently leading to a large measurable magnetization. This approach allows for a revisiting of defect induced magnetism in graphite by eliminating the influence of contamination or artificial effects. We conclude that only spin 1/2 paramagnetism is induced in neutron irradiated graphite. The creation of trans-planar vacancies (without dangling bonds) reduces the concentration of single in-plane vacancies. Complementing our study by first-principles calculations, we propose that both in-plane vacancies and trans-planar defects can form local magnetic moments, which are responsible for the observed 1/2 paramagnetism. The paramagnetism scales up with increasing the amount of defects, however, magnetic order unlikely can occur in a bulk form in defective graphite.

VI. ACKNOWLEDGEMENT

The work was financially supported by the Helmholtz-Gemeinschaft Deutscher Forschungszentren (VH-NG-713 and VH-VI-442). Y. Wang thanks the China Scholarship Council (File No. 2010675001) for supporting his stay at HZDR. The authors also acknowledge the support by the International Science and Technology Cooperation Program of China (2012DFA51430). The Advanced Light Source is supported by the U.S. Department of Energy under Contract No. DE-AC02-05CH11231. Calculations were performed using French HPC resources from the GENCI-CCRT (grant 6194).

- ¹ P. Esquinazi, D. Spemann, R. Höhne, A. Setzer, K.-H. Han, and T. Butz, *Phys. Rev. Lett.* **91**, 227201 (2003).
- ² S. Talapatra, P. G. Ganesan, T. Kim, R. Vajtai, M. Huang, M. Shima, G. Ramanath, D. Srivastava, S. C. Deevi, and P. M. Ajayan, *Phys. Rev. Lett.* **95**, 097201 (2005).
- ³ K. W. Lee and C. E. Lee, *Phys. Rev. Lett.* **97**, 137206 (2006).
- ⁴ H. Xia, W. Li, Y. Song, X. Yang, X. Liu, M. Zhao, Y. Xia, C. Song, T.-W. Wang, D. Zhu, J. Gong, and Z. Zhu, *Adv. Mater.* **20**, 4679 (2008).
- ⁵ J. Červenka, M. I. Katsnelson, and C. F. J. Flipse, *Nat. Phys.* **5**, 840 (2009).
- ⁶ X. Yang, H. Xia, X. Qin, W. Li, Y. Dai, X. Liu, M. Zhao, Y. Xia, S. Yan, and B. Wang, *Carbon* **47**, 1399 (2009).
- ⁷ T. L. Makarova, A. L. Shelankov, I. T. Serenkov, V. I. Sakharov, and D. W. Boukhvalov, *Phys. Rev. B* **83**, 085417 (2011).
- ⁸ Z. He, X. Yang, H. Xia, X. Zhou, M. Zhao, Y. Song, and T. Wang, *Carbon* **49**, 1931 (2011).
- ⁹ N. Shukla, M. Sarkar, N. Banerji, A. K. Gupta, and H. C. Verma, *Carbon* **50**, 1817 (2012).
- ¹⁰ T. Makarova, K.-H. Han, P. Esquinazi, R. da Silva, Y. Kopelevich, I. Zakharova, and B. Sundqvist, *Carbon* **41**, 1575 (2003).
- ¹¹ K.-H. Han, D. Spemann, R. Höhne, A. Setzer, T. Makarova, P. Esquinazi, and T. Butz, *Carbon* **41**, 785 (2003).
- ¹² K.-H. Han, A. Talyzin, A. Dzwilewski, T. L. Makarova, R. Höhne, P. Esquinazi, D. Spemann, and L. S. Dubrovinsky, *Phys. Rev. B* **72**, 224424 (2005).
- ¹³ S. Mathew, B. Satpati, B. Joseph, B. N. Dev, R. Nirmala, S. K. Malik, and R. Kesavamoorthy, *Phys. Rev. B* **75**, 075426 (2007).
- ¹⁴ R. Höhne, P. Esquinazi, V. Heera, and H. Weishart, *Diam. Relat. Mater.* **16**, 1589 (2007).
- ¹⁵ Y. W. Ma, Y. H. Lu, J. B. Yi, Y. P. Feng, T. S. Heng, X. Liu, D. Q. Gao, D. S. Xue, J. M. Xue, J. Y. Ouyang, and J. Ding, *Nature Commun.* **3**, 727 (2012).
- ¹⁶ G. Xing, J. Yi, D. Wang, L. Liao, T. Yu, Z. Shen, C. Huan, T. Sum, J. Ding, and T. Wu, *Phys. Rev. B* **79**, 174406 (2009).
- ¹⁷ S. Zhou, E. Čížmár, K. Potzger, M. Krause, G. Talut, M. Helm, J. Fassbender, S. A. Zvyagin, J. Wosnitza, and H. Schmidt, *Phys. Rev. B* **79**, 113201 (2009).
- ¹⁸ H. Pan, J. B. Yi, L. Shen, R. Q. Wu, J. H. Yang, J. Y. Lin, Y. P. Feng, J. Ding, L. H. Van, and J. H. Yin, *Phys. Rev. Lett.* **99**, 127201 (2007).
- ¹⁹ J. B. Yi, C. C. Lim, G. Z. Xing, H. M. Fan, L. H. Van, S. L. Huang, K. S. Yang, X. L. Huang, X. B. Qin, B. Y. Wang, T. Wu, L. Wang, H. T. Zhang, X. Y. Gao, T. Liu, A. T. S. Wee, Y. P. Feng, and J. Ding, *Phys. Rev. Lett.* **104**, 137201 (2010).
- ²⁰ Y. Liu, G. Wang, S. Wang, J. Yang, L. Chen, X. Qin, B. Song, B. Wang, and X. Chen, *Phys. Rev. Lett.* **106**, 087205 (2011).
- ²¹ M. Roeber, J. Malindretos, A. Bedoya-Pinto, A. Rizzi, C. Rauch, and F. Tuomisto, *Phys. Rev. B* **84**, 081201 (2011).
- ²² M. A. Ramos, J. Barzola-Quiquia, P. Esquinazi, A. Muñoz Martin, A. Climent-Font, and M. Garcia-Hernandez, *Phys. Rev. B* **81**, 214404 (2010).
- ²³ A. Ney, P. Papakonstantinou, A. Kumar, N.-G. Shang, and N. Peng, *Appl. Phys. Lett.* **99**, 102504 (2011).
- ²⁴ R. Nair, M. Sepioni, I.-L. Tsai, O. Lehtinen, J. Keinonen, A. Krasheninnikov, T. Thomson, A. Geim, and I. Grigorieva, *Nature Physics* **8**, 199 (2012).
- ²⁵ M. Sepioni, R. Nair, S. Rablen, J. Narayanan, F. Tuna, R. Winpenny, A. Geim, and I. Grigorieva, *Phys. Rev. Lett.* **105**, 207205 (2010).
- ²⁶ Z. He, X. Yang, H. Xia, T. Z. Regier, D. K. Chevrier, X. Zhou, and T. K. Sham, *Phys. Rev. B* **85**, 144406 (2012).
- ²⁷ L. Li, S. Prucnal, S. D. Yao, K. Potzger, W. Anwand, A. Wagner, and S. Zhou, *Appl. Phys. Lett.* **98**, 222508 (2011).
- ²⁸ Y. Zhang, S. Talapatra, S. Kar, R. Vajtai, S. K. Nayak, and P. M. Ajayan, *Phys. Rev. Lett.* **99**, 107201 (2007).
- ²⁹ M. M. Ugeda, I. Brihuega, F. Guinea, and J. M. Gomez-Rodriguez, *Phys. Rev. Lett.* **104**, 096804 (2010).
- ³⁰ H. Ohldag, P. Esquinazi, E. Arenholz, D. Spemann, M. Rothermel, A. Setzer, and T. Butz, *New J. Phys.* **12**, 123012 (2010).
- ³¹ P. Lehtinen, A. Foster, Y. Ma, A. Krasheninnikov, and R. Nieminen, *Phys. Rev. Lett.* **93**, 187202 (2004).
- ³² P. Esquinazi, J. Barzola-Quiquia, D. Spemann, M. Rothermel, H. Ohldag, N. Garcia, A. Setzer, and T. Butz, *J. Magn. Magn. Mater.* **322**, 1156 (2010).
- ³³ M. Sepioni, R. R. Nair, I.-L. Tsai, A. K. Geim, and I. V. Grigorieva, *EPL (Europhysics Letters)* **97**, 47001 (2012).
- ³⁴ D. Spemann, M. Rothermel, P. Esquinazi, M. A. Ramos, Y. Kopelevich, and H. Ohldag, *EPL (Europhysics Letters)* **98**, 57006 (2012).
- ³⁵ M. Sepioni, R. Nair, I. Tsai, A. Geim, I. Grigorieva, *et al.*, *EPL (Europhysics Letters)* **98**, 57007 (2012).
- ³⁶ D. Spemann, P. Esquinazi, A. Setzer, and W. Böhlmann, *arXiv preprint arXiv:1310.3056* (2013).
- ³⁷ M. Venkatesan, P. Dunne, Y. Chen, H. Zhang, and J. Coey, *Carbon* **56**, 279 (2013).
- ³⁸ M. Sawicki, W. Stefanowicz, and A. Ney, *Semicond. Sci. & Technol.* **26**, 064006 (2011).
- ³⁹ L. M. C. Pereira, J. P. Arajo, M. J. V. Bael, K. Temst, and A. Vantomme, *J. Phys. D-Appl. Phys.* **44**, 215001 (2011).
- ⁴⁰ X. Lin, D. Alber, and R. Henkelmann, *J. Radioanal. Nucl. Chem.* **257**, 531 (2003).
- ⁴¹ E. Wendler, T. Bierschenk, F. Felgenträger, J. Sommerfeld, W. Wesch, D. Alber, G. Bukalis, L. C. Prinsloo, N. van der Berg, E. Friedland, *et al.*, *Nucl. Instr. Meth. Phys. Res. B* **286**, 97 (2012).
- ⁴² B. Kelly, B. Marsden, K. Hall, D. Martin, A. Harper, and A. Blanchard, *IAEA Tecdoc* **1154** (2000).
- ⁴³ P. Bode, *Instrumental and organizational aspects of a neutron activation analysis laboratory*, Ph.D. thesis, Delft University of Technology, Delft (1996).
- ⁴⁴ M. Pimenta, G. Dresselhaus, M. S. Dresselhaus, L. Cancado, A. Jorio, and R. Saito, *Phys. Chem. Chem. Phys.* **9**, 1276 (2007).
- ⁴⁵ I. C. Gerber, A. V. Krasheninnikov, A. S. Foster, and R. M. Nieminen, *New J. Phys.* **12**, 113021 (2010).
- ⁴⁶ A. Arrott, *Phys. Rev.* **108**, 1394 (1957).
- ⁴⁷ E. Wohlfarth, *J. Appl. Phys.* **39**, 1061 (1968).
- ⁴⁸ Z. He, H. Xia, X. Zhou, X. Yang, Y. Song, and T. Wang, *J. Phys. D: Appl. Phys.* **44**, 085001 (2011).

- ⁴⁹ B. Elman, M. Shayegan, M. Dresselhaus, H. Mazurek, and G. Dresselhaus, *Phys. Rev. B* **25**, 4142 (1982).
- ⁵⁰ T. Xing, L. H. Li, L. Hou, X. Hu, S. Zhou, R. Peter, M. Petravic, and Y. Chen, *Carbon* **57**, 515 (2013).
- ⁵¹ R. Telling and M. Heggie, *Philosophical Magazine* **87**, 4797 (2007).
- ⁵² T. Makarova, M. Riccò, D. Pontiroli, M. Mazzani, M. Belli, and A. Goffredi, *physica status solidi (b)* **245**, 2082 (2008).
- ⁵³ T. Jawhari, A. Roid, and J. Casado, *Carbon* **33**, 1561 (1995).
- ⁵⁴ H. Ohldag, T. Tyliczszak, R. Höhne, D. Spemann, P. Esquinazi, M. Ungureanu, and T. Butz, *Phys. Rev. Lett.* **98**, 187204 (2007).
- ⁵⁵ P. O. Lehtinen, A. S. Foster, Y. Ma, A. V. Krasheninnikov, and R. M. Nieminen, *Phys. Rev. Lett.* **93**, 187202 (2004).
- ⁵⁶ O. V. Yazyev, *Phys. Rev. Lett.* **101**, 037203 (2008).
- ⁵⁷ R. Telling, C. Ewels, A. El-Barbary, and M. Heggie, *Nat. Mater.* **2**, 333 (2003).
- ⁵⁸ E. Machado-Charry, P. Boulanger, L. Genovese, N. Mousseau, and P. Pochet, *Appl. Phys. Lett.* **101**, 132405 (2012).
- ⁵⁹ S. Krishnan, G. Brenet, E. Machado-Charry, D. Caliste, L. Genovese, T. Deutsch, and P. Pochet, *Appl. Phys. Lett.* **103**, 251904 (2013).
- ⁶⁰ L. Genovese, A. Neelov, S. Goedecker, T. Deutsch, S. A. Ghasemi, A. Willand, D. Caliste, O. Zilberberg, M. Rayson, A. Bergman, and R. Schneider, *J. Chem. Phys.* **129** (2008).
- ⁶¹ L. Genovese, T. Deutsch, and S. Goedecker, *J. Chem. Phys.* **127** (2007).
- ⁶² O. V. Yazyev and L. Helm, *Phys. Rev. B* **75**, 125408 (2007).
- ⁶³ J. Barzola-Quiquia, P. Esquinazi, M. Rothermel, D. Spemann, T. Butz, and N. García, *Phys. Rev. B* **76**, 161403 (2007).